Geochemistry Geophysics Geosystems G3

Article
Volume 11, Number 8
11 August 2010
Q08011, doi:10.1029/2010GC003091
ISSN: 1525-2027

Published by AGU and the Geochemical Society

Spatial variations of crustal characteristics beneath the Hoggar swell, Algeria, revealed by systematic analyses of receiver functions from a single seismic station

Kelly H. Liu and Stephen S. Gao

Department of Geological Sciences and Engineering, Missouri University of Science and Technology, 129 McNutt Hall, Rolla, Missouri 65409, USA (liukh@mst.edu; sgao@mst.edu)

[1] The Hoggar swell in Algeria is one of the significant massifs of northwest Africa. The paucity of high-resolution geophysical studies of the crust and mantle beneath the massifs is mostly responsible for the heated debates about the depth of the source region of the Cenozoic volcanism and the closely related uncertainty about the mechanism that formed and maintains the high elevation of the swells. Here we report results from a systematic study of 1386 high-quality receiver functions (RFs) recorded by station TAM, the only permanent broadband seismic station on the Hoggar swell. The resulting crustal thickness is about 34 km and the V_p/V_s is 1.77 when all the RFs from the station are stacked. Our study reveals a sharp contrast in the amplitude of the *P*-to-*S* converted phases between the volcanic, highly-fractured Tefedest terrane and the non-volcanic, less fractured Laouni terrane. The former has a stacking amplitude that is comparable to typical cratonic areas, and the latter has an amplitude that is only about 25% as large. Spatially consistent crustal thickness and an intermediate-mafic crust are inferred on the Tefedest terrane, while spatially variable crustal thickness and a felsic crust is inferred beneath the Laouni terrane. The observations can be best explained by a mantle-derived underplated magmatic layer beneath the mechanically-stronger Laouni terrane, and magmatic diking and resultant volcanism associated with the mechanically weaker Tefedest crust. The study demonstrated the significance of a long-running station in the investigation of spatial variations of crustal characteristics.

Components: 7700 words, 11 figures.

Keywords: Hoggar swell; mantle plume; receiver function; continental crust; magmatism; Moho.

Index Terms: 7205 Seismology: Continental crust (1219); 7208 Seismology: Mantle (1212, 1213, 8124); 7218 Seismology: Lithosphere (1236).

Received 17 February 2010; **Revised** 7 June 2010; **Accepted** 11 June 2010; **Published** 11 August 2010.

Liu, K. H., and S. S. Gao (2010), Spatial variations of crustal characteristics beneath the Hoggar swell, Algeria, revealed by systematic analyses of receiver functions from a single seismic station, *Geochem. Geophys. Geosyst.*, *11*, Q08011, doi:10.1029/2010GC003091.

1. Introduction

[2] Northwest Africa is host to a number of topographic highs topped with Cenozoic, dominantly basaltic volcanism (Figure 1). Those swells are similar in terms of age, dimensions, amplitude of gravity anomalies, and volcanic activities [*Liegeois et al.*, 2005; *Doucoure and de Wit*, 2003]. While swells with comparable characteristics are commonly found on ocean floors, a simple comparison

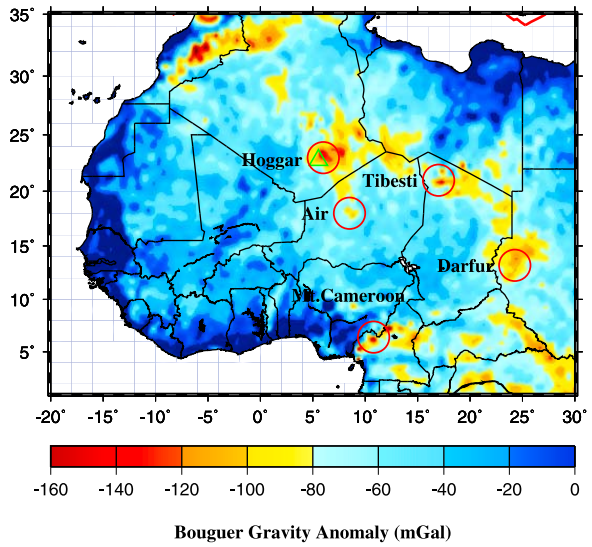

Figure 1. Bouguer gravity anomalies of northwest Africa computed using the GRACE (Gravity Recovery and Climate Experiment) satellite gravity data [*Tapley et al.*, 2005], the GTOPO-30 topographic model, and a mean crustal density of 2.67 g/cm^3. Circles represent major Cenozoic volcanic swells.

of global elevation, Bouguer gravity, seismicity, and Cenozoic volcano distribution maps suggests that northwest Africa is perhaps the only "stable" continental area with such large-scale swells on Earth. Both plume [e.g., *Sleep*, 1990; *Burke*, 1996] and non-plume [e.g., *Ayadi et al.*, 2000; *Liegeois et al.*, 2005; *Beccaluva et al.*, 2007] hypotheses have been proposed for the formation of the swells. The debate is mostly caused by a paucity of high-resolution geophysical (especially broadband seismic) studies of the crustal and mantle structure beneath the swells.

1.1. Geological Setting of the Hoggar Swell

[3] The Hoggar swell is the largest among the several volcanic swells in northwest Africa (Figure 1). Stratigraphic records suggest that this area was already a topographic high during the Cretaceous time [*Liegeois et al.*, 2005]. The study area is located in central Hoggar and consists of the Tefedest and the Laouni terranes (Figure 2) [*Black et al.*, 1994]. Tectonically, it is part of the Tuareg shield, which was formed through accretion events at about 600 Ma [*Liegeois et al.*, 2003, 2005]. The oldest basement rocks are Archean in age [*Peucat et al.*, 2003]. Three main phases of Cenozoic volcanism have been identified on the Hoggar swell, including the Upper Eocene to Oligocene, Miocene to Mio-Pliocene, and Late Pliocene to late Quaternary episodes [*Liegeois et al.*, 2005]. The dominantly basaltic lavas have rare earth element patterns that are similar to ocean island basalts, and cover a layer of about 100 m thick in several volcanic districts in Central Hoggar [*Liegeois et al.*, 2005] (Figure 2). Geochemical analyses of mantle xenoliths suggest that the Cenozoic volcanism might be related to rejuvenation and thinning of the lithosphere by asthenospheric upwelling, which could be induced by the large difference in lithospheric thickness between the Hoggar swell and the cratonic area to the west [*Beccaluva et al.*, 2007].

[4] The NE-SW striking fault that separates the two terranes is a member of the conjugate brittle fault system formed by the indentation of the West African craton during the Pan-African orogeny at about 500–600 Ma (Figure 2) [*Ball*, 1980]. The southwestern end of the fault is the continental-scale N-S oriented 4°50′ fault, at a distance of about 95 km from the center of the study area (Figure 2). It represents the sharp eastern boundary of the Tahalra volcanic field on the Tefedest terrane, in which the latest eruption was as recent as the historical time [*Assouni-Sekkal et al.*, 2007]. Relative to the Laouni terrane, the Tefedest has a much better developed brittle fault system (Figure 2) [*Ball*, 1980; *Liegeois et al.*, 2005]. The obvious role of the fault on the spatial distribution of volcanism suggests that it is a deep fault, perhaps

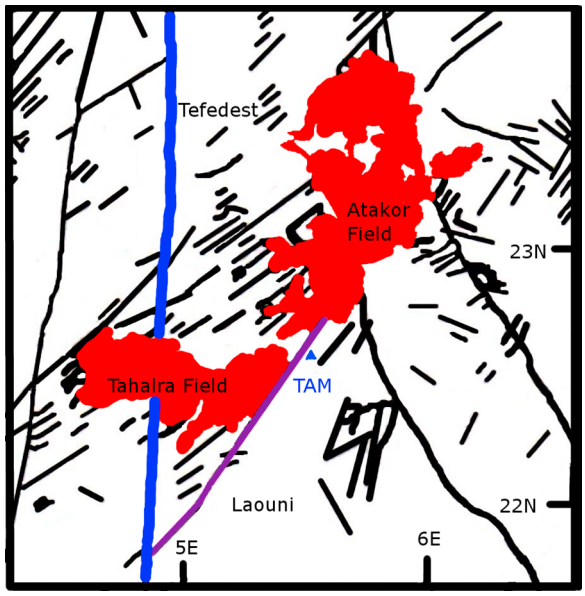

Figure 2. Distributions of Cenozoic volcanism (red areas) and brittle fracture systems in central Hoggar. The purple line represents the fault separating the Tefedest and Laouni terranes, the blue N-S line represents the 4°50′ fault, and the blue triangle is seismic station TAM (modified based on *Liegeois et al.* [2005]).

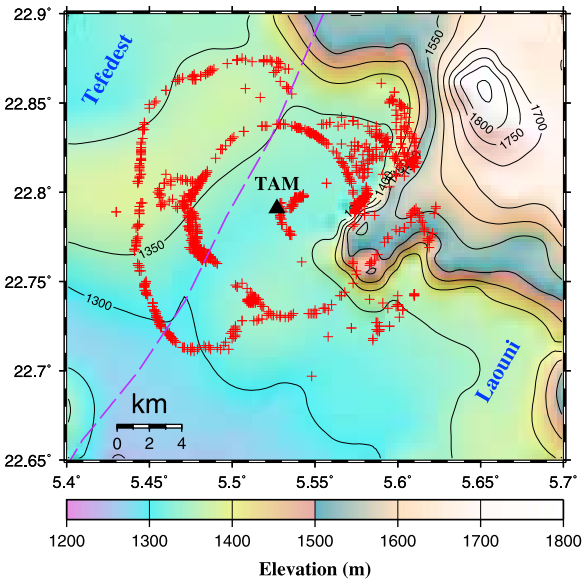

Figure 3. Surface topography of the study area and distribution of ray-piercing points of the P_mS phase at 35 km depth (pluses). The dashed line represents the fault separating the Tefedest and Laouni terranes. The fault was digitized based on Google Earth images.

lithospheric in nature, although the mechanism for the fault to control the spatial distribution of the volcanism remains unresolved.

1.2. Results of Previous Geophysical Studies

[5] By applying a grid-search modeling technique, *Sandvol et al.* [1998] found a crustal thickness of 38 ± 0 km using 14 events recorded by station TAM, data from which are used in the current study. *Sandvol et al.* [1998] concluded that the crustal structure beneath the station is very homogeneous. Similarly, under the assumption of a laterally homogeneous crust, *Gangopadhyay et al.* [2007] revealed a crustal thickness of 36 km and a *P*-and *S*-wave velocity range of 6.25–6.8 km/s and 3.1–3.9 km/s, respectively, using data from 6 events. As shown below, our results suggest a dramatic contrast in *Moho* characteristics between the Tefedest and Laouni terranes sampled by the 1386 events used in the study, highlighting the importance of additional data and that of a data analysis approach that is beyond the common assumption of laterally homogeneous crust beneath a station.

[6] Seismic *P*-wave tomography inversion using data from a 2.5 month deployment of 33 short-period vertical seismometers across central Hoggar [*Ayadi et al.*, 2000] found that in the top 100 km, the seismic *P*-wave velocity beneath the study area is a few percent lower than that beneath the Sahara basin located to the north of the Hoggar swell. Within the study area (Figure 3), the crustal velocity beneath the Tefedest terrane is 1–2% higher than that beneath the Laouni terrane [*Ayadi et al.*, 2000]. As shown below, these observations, when combined with results from this study, suggest a sharp contrast in crustal mechanical strength and its resulting control on magmatic movement between the two terranes.

[7] Under the assumption of isostatic balance, the large swell must be underlain by a lower density anomaly in the crust and/or mantle. Nevertheless, conflicting results exist regarding the density structure of the crust and mantle beneath the Hoggar swell from investigations of gravity anomalies. *Brown and Girdler* [1980] attributed the negative Bouguer gravity anomaly associated with the swell to an approximately 40 km thinning of an assumed 100 km thick original lithosphere, i.e., the lighter layer is in the depth range of 60–100 km. This is inconsistent with other gravity studies such as that of *Crough* [1981] who inferred the existence of a magmatic body at the depth shallower than 60 km, or that of *Lesquer et al.* [1988] who suggested that the magmatic body exists in the depth range of 20 to 70 km with a thickness that is 30 km or thinner.

[8] Based on seismic tomography and gravity inversion results and the observation that the Hoggar swell is not associated with significant high-heat-flow anomalies [*Lesquer et al.*, 1989], *Liegeois et al.* [2005] suggested that there is no thinning of the lithosphere beneath Hoggar and that the source of the observed negative gravity anomaly must reside at a depth of 250 km or greater. They also proposed that the volcanism in Hoggar and other northwest Africa swells (Figure 1) is not related to mantle plumes, but instead is the results of rejuvenation of Pan-African structures and has an upper-lithospheric source. On the other hand, some low-resolution seismic tomography results revealed a deep low-velocity column beneath Hoggar, e.g., the global-scale shear-wave velocity model of *Grand* [2002] (as referenced by *Begg et al.* [2009]) suggested a column of lower shear-velocity with a radius of about 500 km at most depth ranges, extending to a depth of greater than 1000 km.

[9] Some of the major remaining unresolved questions on the Hoggar swell (and most other swells in

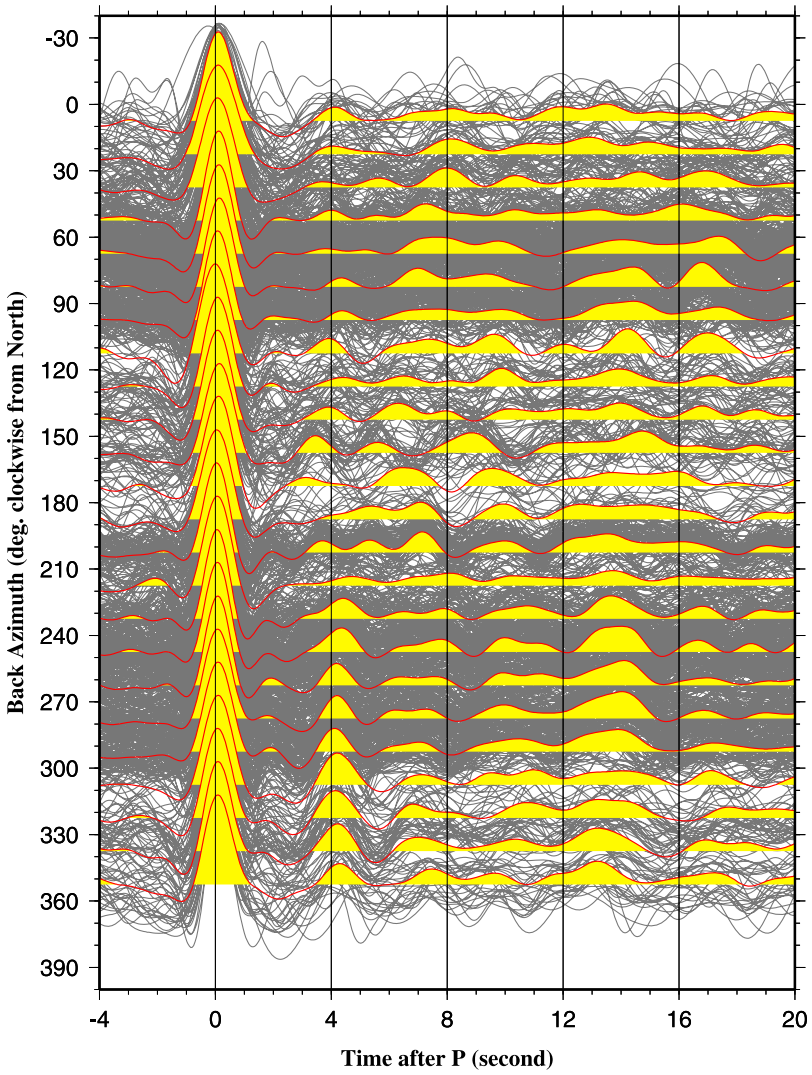

Figure 4. Radial receiver functions used in the study plotted against the back-azimuth of each event. Gray thin lines are individual RFs, and red thick lines are stacked RFs in 15° azimuthal bins.

northwest Africa) are the depth of the source area of the volcanic rocks, the closely-related question of the mechanism for magma generation, and the relationship between the swells and the African superplume observed in the lower mantle beneath southern Africa [e.g., *Garnero et al.*, 2007]. The answers to those questions may provide key constraints on the more fundamental problems such as the mechanism that caused and maintains the high elevation of the swells. Here we present results of systematic analyses of *P*-to-*S* converted (P_xS which includes P_mS and its multiples PP_mS and PS_mS) phases at the *Moho* by stacking receiver functions (RFs) recorded over a 20 year period by station TAM on the Hoggar swell, aiming at proposing an explanation of the intriguing distribution of Cenozoic volcanism (Figure 2) and providing constraints on the source depth of the volcanism.

2. Data and Methods

[10] The broadband seismic data used in the study were recorded by GEOSCOPE station TAM (latitude: 22.7915°, Longitude: 5.5284°, Elevation: 1410 m), which is located in the city of Tamanrasset, a provincial capital of about 60,000 inhabitants in southern Algeria. The station has been almost continuously providing broadband, high-gain data since early 1990. Data from teleseismic events in the epicentral distance range of 30° to 180° were requested from the IRIS (Incorporated Research Institutions

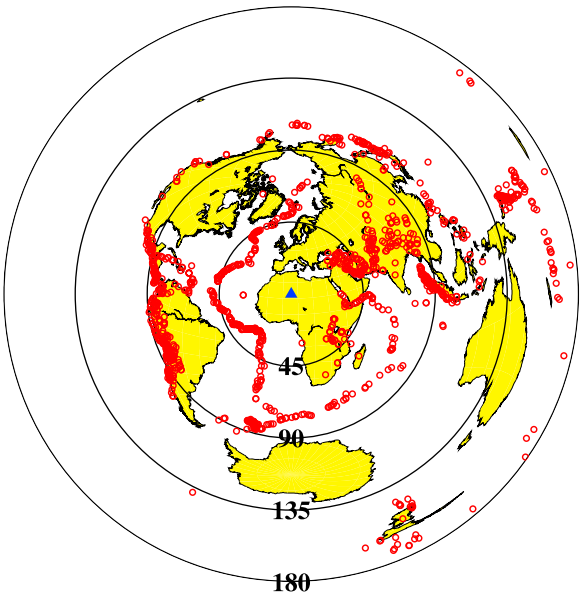

Figure 5. An azimuthal-equidistant projection map centered at station TAM (triangle) showing the distribution of earthquakes used in the study. The numbers indicate distance (in degree) from the station.

for Seismology) DMC (Data Management Center). The cut-off magnitude is determined using $M_c = 5.2 + (D_e - 30.0)/(180.0 - 30.0) - H_f/700$, where D_e is the epicentral distance in degree, and H_f is the focal depth in km. The resulting M_c ranges from 4.2 (for events with $D_e = 30°$ and $H_f = 700$ km) to 6.2 (for events with $D_e = 180°$ and $H_f = 0$ km). The parameters used in the equation are the results of extensive tests and represent the optimal balance between the quantity and quality of the data to be requested. Broadband, high-gain data from 3958 events that satisfy the above epicentral distance and M_c criteria were obtained from the IRIS DMC for the period of 3/12/1990 to 12/19/2009. The seismograms were windowed to begin at 20 s before and 260 s after the first compressional waves (which include P, P_{diff}, and PKP and are collectively called P-waves herein) computed based on the IASP91 earth model.

[11] We next band-pass filter the seismograms using a 4-pole, 2-pass Butterworth filter with corner frequencies 0.08–0.8 Hz to enhance the signal, and select the events with a signal to noise ratio (S/N) of 4.0 or greater on the radial component. The S/N is calculated using $S = \max|A_s|/|\overline{A}_n|$, where $\max|A_s|$ is the maximum absolute value on the seismogram in the time window of 8 s before and 12 s after the predicted IASP91 arrival time for the first P-wave, and $|\overline{A}_n|$ is the mean absolute value on the seismogram in the time window of 5–15 s before the predicted arrival time. The above automatic selection process resulted in 2050 events with high S/N. Those seismograms were converted into radial RFs using the procedure of *Ammon et al.* [1990]. The RFs were examined visually to reject those with weak first P-arrivals or with anomalously large arrivals in the P-wave coda. A total of 1386 radial RFs were chosen for the study (Figure 4). Note that the number of high-quality RFs from this single permanent station is comparable with the total number of RFs from most large-scale portable seismic experiments. For instance, the Kaapvaal craton seismic experiment, which was one of the largest portable seismic experiments ever conducted, occupied about 80 sites over a 2-year period and produced a total of 1544 usable RFs [*Nair et al.*, 2006]. Because the station is located near the center of the "land hemisphere," which is mostly surrounded by plate boundaries, an excellent azimuthal coverage by the high-quality events is obtained (Figure 5). The geographic coordinates of the ray-piercing points of P_mS at 35 km depth (Figure 3) were calculated using the ray-parameter of the direct P-wave, a crustal P-wave velocity of 6.5 km/s, and a V_p/V_s of 1.77.

[12] $H - \kappa$ (i.e., thickness-V_p/V_s) stacking of receiver functions [*Zhu and Kanamori*, 2000] is a well-tested, effective tool to measure crustal thickness and V_p/V_s which is directly related to the more commonly known Poisson's ratio (γ) by the relationship $\gamma = 0.5[1 - 1/(\phi^2 - 1)]$, where $\phi = V_p/V_s$. Previous RF and laboratory studies demonstrated that more mafic rocks have higher V_p/V_s [*Christensen*, 1996]. The mean V_p/V_s value for granitic, andesitic, and basaltic rocks is 1.71, 1.78, and 1.87, respectively [*Tarkov and Vavakin*, 1982]. Laboratory experiments suggest that V_p/V_s is about 1.74 for the upper crust and about 1.81 for the lowermost crust, resulting in a mean crustal V_p/V_s of 1.78 [*Christensen*, 1996]. In this study we use the method of *Zhu and Kanamori* [2000] to stack the P_xS phases to search for the optimal crustal thickness and V_p/V_s. Details of the procedure are given by *Nair et al.* [2006], who proposed a third parameter, R, the stacking amplitude, to quantify the effectiveness of the *Moho* in producing P_xS phases.

[13] We use the bootstrap resampling approach [*Efron and Tibshirani*, 1986; *Press et al.*, 1992] to compute the mean values of H, V_p/V_s, and R and to estimate their standard deviations (STDs). For each of the 20 bootstrap steps, we randomly select

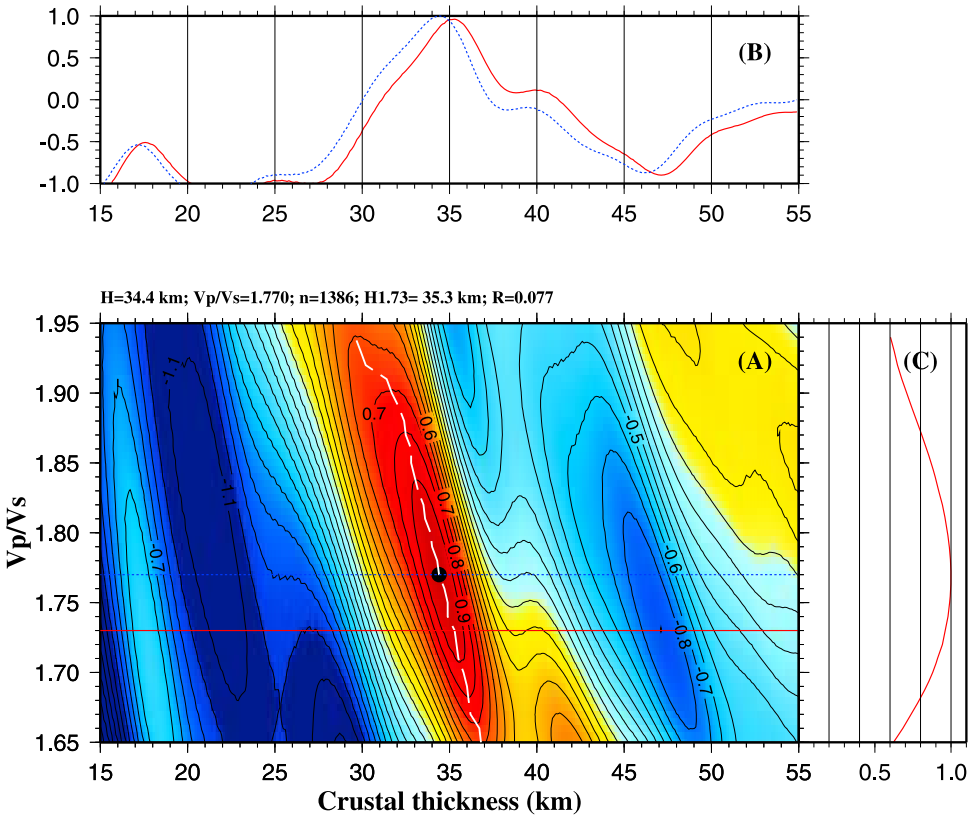

Figure 6. (a) $H - \kappa$ plot using all the high-quality radial RFs recorded by station TAM. (b) The red line shows stacking amplitudes for V_p/V_s = 1.73 (which is the mean V_p/V_s for crustal rocks), and the blue line shows stacking amplitudes for the optimal V_p/V_s. (c) Stacking amplitude along the dashed white line in Figure 6a, demonstrating the significance of the peak which is marked by the black dot in Figure 6a.

1-1/e ≈ 63% independent RFs to form RF Gather A. We then randomly choose 60% of the RFs in Gather A to form Gather B. The two gathers are combined to form Gather C which has the same number of RFs as that in the original data set (63% + 0.6 * 63% ≈ 100%). RFs in Gather C are then used to produce H, V_p/V_s, and R observations for the bootstrap step.

[14] In southern Africa results from a study using the same techniques as in this study [*Nair et al.*, 2006] suggest that the relatively undisturbed Precambrian cratonic areas have felsic crust with a V_p/V_s in the range of 1.70–1.74 and a R value in the range of 0.15–0.25. Significantly larger V_p/V_s values (1.78–1.82) and smaller R values (0.05–0.10) are found beneath the Bushveld mafic intrusion complex. Those observations, together with the observation that there is a 10 km thickening of the crust beneath the Bushveld, were interpreted by *Nair et al.* [2006] as the evidence for underplating of a mafic layer and intensive dikes in the crust. Those observations will be compared with results presented below to infer crustal characteristics beneath the Hoggar swell.

3. Results

3.1. Overall Crustal Properties

[15] To obtain a first-order estimate of H, V_p/V_s, and R, we apply the $H - \kappa$ stacking technique to stack all the radial RFs recorded by TAM together. The searching interval for H is 0.1 km, and that for V_p/V_s is 0.01. The weighting factors are 0.5 for *PmS*, 0.4 for *PPmS*, and 0.1 for *PSmS* (see *Zhu and Kanamori* [2000] and *Nair et al.* [2006] for details about the weighting factors). A well-defined peak on the $H - \kappa$ plot (Figure 6) is found. The bootstrap approach using all the 1386 RFs yields a crustal thickness of 34.4 ± 0.1 km, a V_p/V_s of 1.772 ± 0.004, and a R of 0.0791 ± 0.002 when an average crustal P-wave velocity of 6.5 km/s is used. The

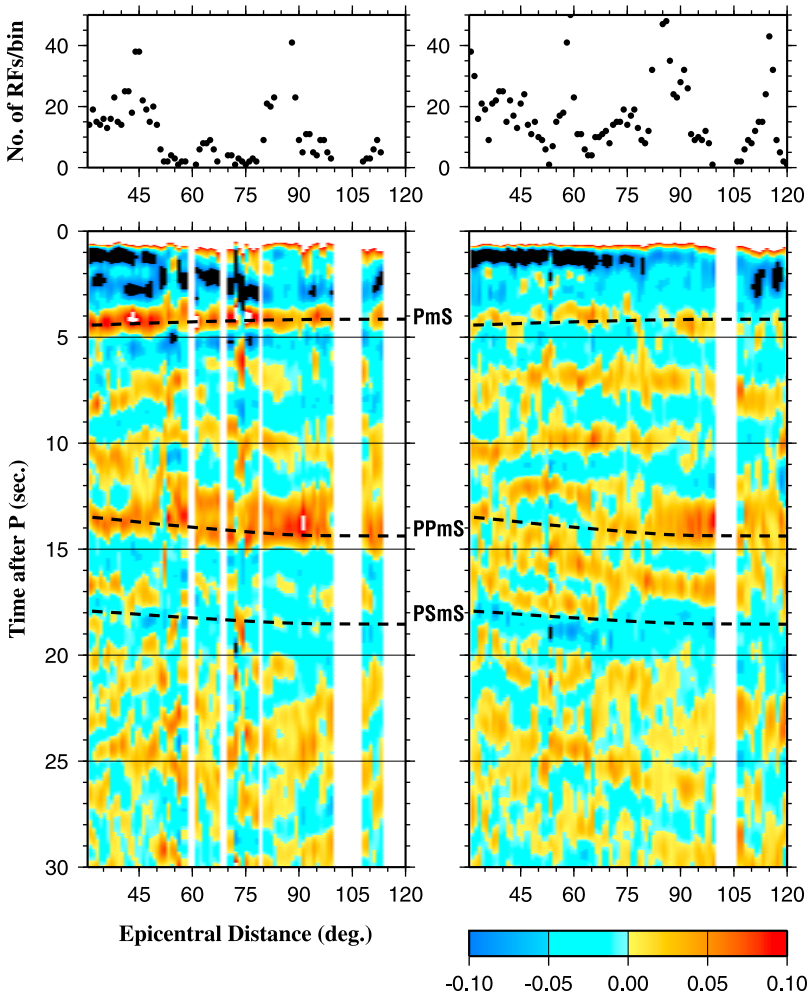

Figure 7. (bottom) Stacked RFs in epicentral distance bins and (top) the number of RFs per bin. Figure 7 (left) shows results with ray-piercing points in the Tefedest terrane, and Figure 7 (right) shows results with ray-piercing points in the Laouni terrane. Dished lines are predicted arrival times for *PmS*, *PPmS*, and *PSmS*, respectively. The scale bar shows the amplitude relative to that of the direct *P*-wave.

crustal thickness is similar to that obtained by *Sandvol et al.* [1998] and *Gangopadhyay et al.* [2007], and is almost identical to the value used by *Ayadi et al.* [2000] in their tomographic inversion. The crustal *P*-wave velocity of 6.5 km/s is chosen based on active-source seismic surveys conducted in stable parts of Africa such as the Kaapvaal craton [*Durrheim and Green*, 1992] and the average crustal *P*-wave velocity from the RF studies of *Sandvol et al.* [1998] and *Gangopadhyay et al.* [2007].

[16] As demonstrated using synthetic seismograms [*Nair et al.*, 2006], the resulting H measurements decrease and the V_p/V_s values increase almost linearly with the difference between the velocity used for stacking and the actual velocity. For instance, in our study area, the results are (31.3 km, 1.79), and (37.7 km, 1.75) when a crustal V_p of 6.0 and 7.0 km/s is used, respectively, although such large departures are unlikely. Those values show that even when an unreasonably large crustal V_p of 7 km/s is used, the averaged V_p/V_s over all the areas sampled by the RFs suggests that the crust in the vicinity of the station is more mafic than the less modified southern part of the Kaapvaal craton, which was found to have a thickness of about 35 km and a V_p/V_s of about 1.72 when a crustal velocity of 6.5 km/s is used [*Nair et al.*, 2006].

3.2. Differences in Crustal Properties Between the Tefedest and Laouni Terranes

[17] Figure 4 shows stacks of the RFs in 15° azimuthal bands. Those stacks, which are simple time-

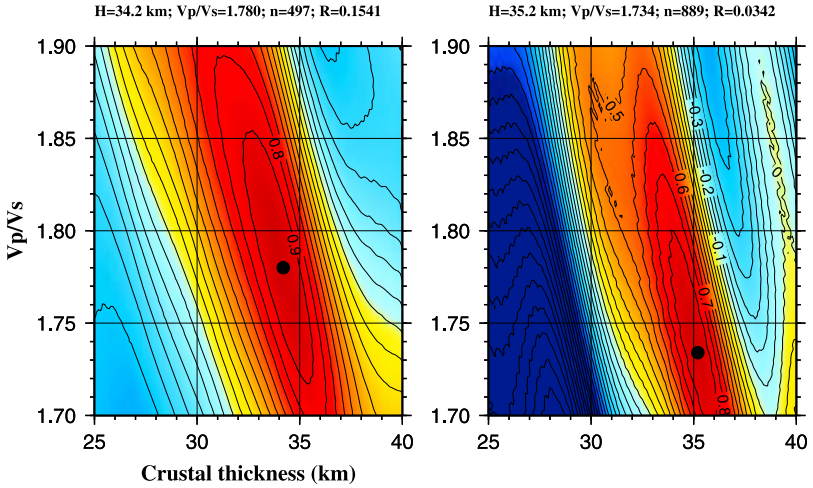

Figure 8. Results of $H - \kappa$ stacking using all the RFs in the (left) Tefedest and (right) Laouni terranes. Note the large difference in the resulting R values shown at the top.

domain summations without taking into account of the differences in ray-parameters among the events with different epicentral distances, suggest clear and systematic variations in crustal thickness and especially the amplitude of the P_mS phase at about 4 s after the first P-arrivals, indicating significant spatial variations in crustal thickness and the effectiveness of the *Moho* in producing P_xS phases. For those in the back-azimuth range of 230°–360° (i.e., events from the southwest – north), a strong arrival, which is most likely the P_mS phase, is observed at about 4.2 s after the direct P-wave. The amplitude of this phase is greatly reduced for events from the other azimuthal bands, and the arrival times vary from about 3.5 s to over 5 s. The ray-piercing points of the former group are mostly located on the northwest side of the fault separating the Tefedest and the Laouni terranes, and those for the latter group are on the southeast side of the fault (Figure 3).

[18] We next group the RFs into (focal-depth corrected) epicentral distance bins of 2° wide with a 1° overlap among neighboring bins, and stack those in the same bins (Figure 7). The amplitudes of the P_xS phases of the RFs with piercing points in the Tefedest terrane are significantly larger than those in the Laouni terrane. In addition, the actual arrival times of the three phases match reasonably well with the predicted times, which were computed using a crustal thickness of 34.4 km, V_p of 6.5 km/s, and V_p/V_s of 1.77. Those observations suggest that to the first order, the crustal thickness beneath the two terranes is similar, and the major difference is the amplitude of the converted phases. The epicentral-distance-based stacking also demonstrates that the RFs with piercing points in the two terranes have similar epicentral distance distributions (Figure 7, top), suggesting that the difference in the amplitudes of the converted phases is not caused by differences in the incidence angle of the raypaths.

[19] The similarities and differences in crustal characteristics between the two terranes are additionally demonstrated by the $H - \kappa$ stacking results using RFs with ray-piercing points in the two terranes separately (Figure 8). We applied the bootstrap approach to the RFs with ray-piercing points on the Tefedest terrane and found a crustal thickness of 34.2 ± 0.1 km and a V_p/V_s of 1.781 ± 0.002. For the RFs on the Laouni terrane, the corresponding values are 34.8 ± 0.2 km and 1.750 ± 0.009. The V_p/V_s observations suggest that the Tefedest terrane is characterized by a intermediate-mafic crust and the Laouni terrane is underlain by a felsic crust. The stacking amplitude is 0.156 ± 0.003 for the Tefedest terrane and 0.037 ± 0.003 for the Laouni terrane which is merely 25% of that observed in the former terrane. Note that the stacking amplitude for the Tefedest terrane is similar to those observed on most cratonic areas such as the Kaapvaal craton [*Nair et al.*, 2006].

3.3. Spatial Distribution of Crustal Properties

[20] We search for possible systematic spatial variations of the crustal thickness, crustal V_p/V_s, and stacking amplitude by stacking RFs in a series of

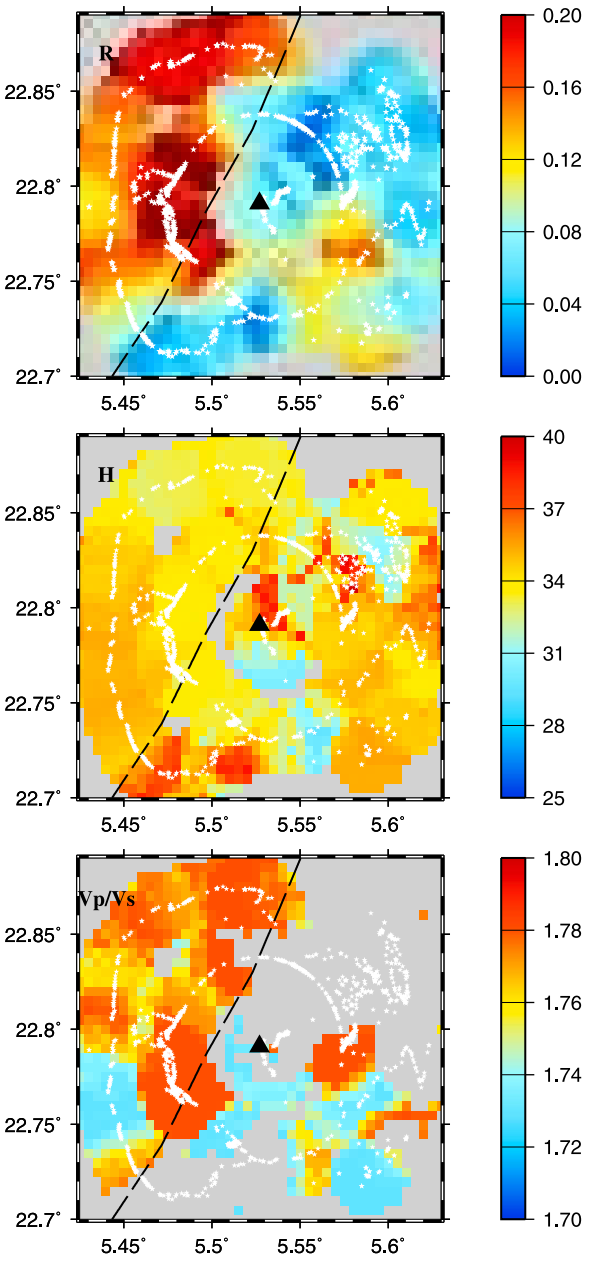

Figure 9. Spatial distribution of (top) mean stacking amplitude, (middle) crustal thickness in km, and (bottom) V_p/V_s observations derived from bootstrap analyses. For Figure 9 (bottom), only nodes with $R \geq 0.08$ are plotted. White stars are P_mS ray-piercing points at the depth of 35 km.

circular areas. We first sample the study area by a network of evenly spaced nodes with a distance between neighboring nodes of 0.005° (about 0.5 km). For each node, we perform 20 bootstrap $H - \kappa$ stacking steps using a set of maximum 30 RFs with the smallest distance between the ray-piercing points and the node. The maximum searching distance allowed is 0.02° (about 2 km) in order to ensure coherency among the RFs to be stacked. A node is not used in the final mapping if the number of RFs within the circle is less than 5.

[21] The stacking uses a crustal V_p of 6.5 km/s, a 25–40 km searching range for H, and a 1.73–1.79 range for V_p/V_s. For nodes with a small stacking amplitude, the uncertainty in the resulting H and especially in V_p/V_s is unavoidably large. In order to display only the nodes with the most reliable results, we use a cutoff stacking amplitude of R_c = 0.08 which is approximately half of the amplitude observed in typical cratonic areas. For nodes with $R \geq R_c$, the optimal H and V_p/V_s are displayed in Figure 9; and for nodes with $R < R_c$, the V_p/V_s is not displayed and the H values displayed are those corresponding to V_p/V_s = 1.77 which is the overall V_p/V_s beneath the station. The mean parameters over the bootstrap steps for each of the nodes are shown in Figure 9, and their STDs are shown in Figure 10. The average of the STDs over all the blocks is 0.0132 for R, 1.0 km for H, and 0.007 for V_p/V_s, suggesting that for most of the nodes, the resulting parameters especially the R and H values are well-defined.

[22] The resulting spatial distribution of the stacking amplitudes (Figure 9, top) re-enforces the preliminary observation that the fault, which separates the volcanic Tefedest terrane and the non-volcanic Laouni terrane in the study area, is also the boundary between high and low stacking amplitudes. In addition, the crustal thickness beneath the Tefedest terrane is almost uniform, while that beneath the Laouni terrane varies significantly. Most part of the Tefedest terrane is characterized by a V_p/V_s of about 1.78, while the V_p/V_s in the Laouni terrane is lower and more variable.

4. Discussion

4.1. Magmatic Underplating as a Possible Cause for the Small Stacking Amplitudes in the Laouni Terrane

[23] The most robust result from the study is the dramatic contrast in stacking amplitudes between the Tefedest and Laouni terranes which are separated by a presumably lithospheric fault (Figure 9). In spite of its intensive brittle fault system and widespread Cenozoic volcanism (Figure 2), the Tefedest terrane demonstrates large R values that are similar to the relatively undeformed part of typical cratons such as the southern Kaapvaal craton. On the other

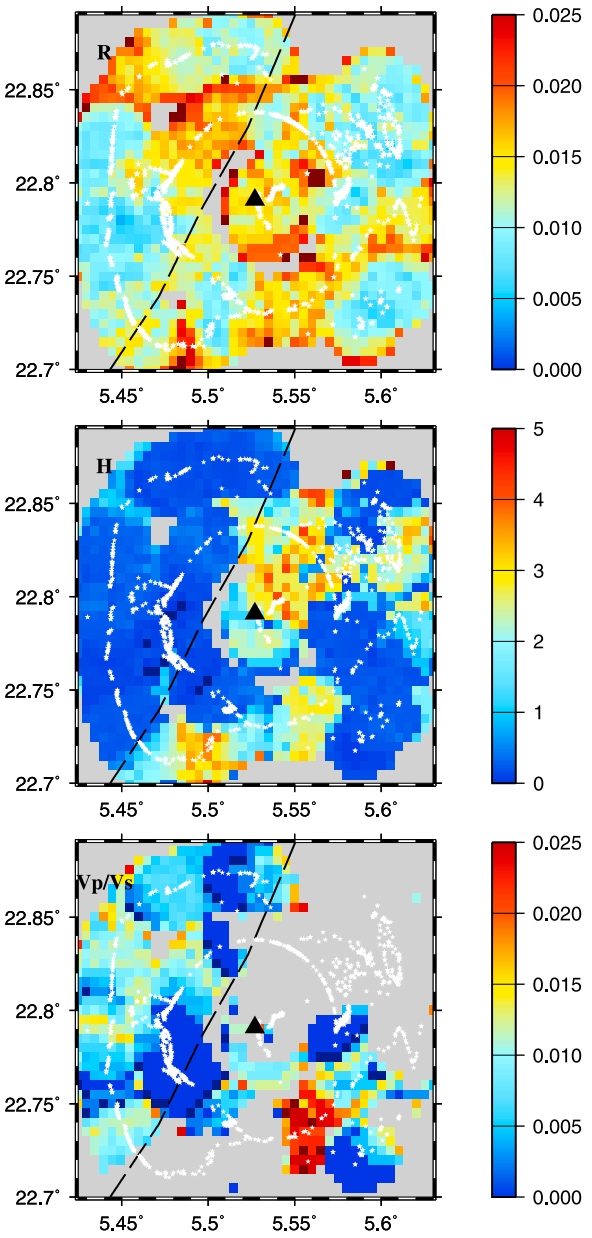

Figure 10. Spatial distribution of bootstrap-derived STDs for (top) stacking amplitude, (middle) crustal thickness in km, and (bottom) V_p/V_s.

hand, the R values on the apparently less deformed and non-volcanic Laouni terrane are extremely small.

[24] The observed spatial variation of R has several possible causes. The first is lateral velocity variations in the crust. Such variations lead to departure of predicted and actual arrival times of the *Moho* phases, resulting in incoherent stacking and thus reduction in stacking amplitude. However, as argued by *Nair et al.* [2006], under reasonable assumptions about the magnitude of the velocity heterogeneities, the amount of the departure is several times smaller than the dominant period of the P_xS phases and thus this factor cannot account for the observed large difference in R between the two terranes. In addition, if crustal velocity heterogeneities are the cause of the difference, one would have to reach the unlikely conclusion that the crust beneath the volcanic Tefedest terrane is much more homogeneous than the non-volcanic Laouni terrane. The second possible cause is the sharpness of the *Moho*, i.e., the vertical distance (z) over which the transition from crustal ($V_p \approx 6.5$ km/s) to mantle ($V_p \approx 8.1$ km/s) velocities takes place. Synthetic studies [e.g., *Poppeliers and Datta*, 2010] demonstrate that the amplitude of the P_xS phases will reduce for increased z. While this could suggest that the small stacking amplitudes observed on the Laouni terrane are the results of a blurred Moho, the synthetic studies also reveal greatly broadened P_xS phases corresponding to the reduced amplitude. This correspondence is not observed. Instead, the P_mS phases on the Laouni terrane are as sharp as those on the Tefedest terrane (Figure 4), suggesting that *Moho* sharpness is not the main cause of the observed contrast in R. The third possible cause is subwavelength-scale *Moho* topography which causes scattering of the converted phases and consequently reduces their amplitudes. Synthetic tests [*Poppeliers and Datta*, 2010] suggest that when the intensity of such topography is high enough to cause significant reduction in the amplitude of the P_xS phases, it should also introduce observable noise around the P_mS phase. This is inconsistent with the simple RF waveforms for both terranes (Figure 4). Thus small-scale *Moho* topography is unlikely a cause of the observed spatial distribution of the stacking amplitude.

[25] Our favorite model for the small R values observed on the Laouni terrane involves a mantle-derived mafic layer between the original crust and mantle (Figure 11). This layer, which most likely has a seismic velocity that is between that of the crust and mantle, has the capability of significantly reducing the velocity contrast across the *Moho*, and thus reduces the amplitude of the P_xS phases. Although a mafic layer above the *Moho* with a velocity that is similar to that of the upper-most mantle can also reduce the amplitude by reducing the velocity contrast across the *Moho*, it would also lead to an increase in the mean V_p/V_s of the Laouni crust. Such an increase is not observed in the Laouni terrane. On the contrary, a slightly decrease in V_p/V_s relative to the volcanic Tefedest terrane is observed (Figures 8 and 9), suggesting that the

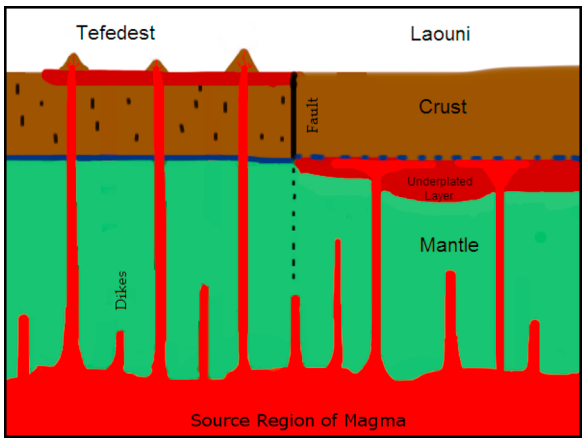

Figure 11. A schematic diagram showing the structure of the upper lithosphere beneath the study area. Vertical bars in the Tefedest crust represent fractures in the mechanically weaker crust.

mantle-derived mafic layer is beneath the *Moho* and thus belongs to the mantle.

[26] If the velocity contrast across the bottom of the underplated layer is high enough, the transition from the "normal" mantle to the underplated layers is sharp enough, and the thickness of the layer is greater than the wavelength of the *P*-to-*S* converted phase (about 10 km), a positive *P*-to-*S* converted phase should be observed on the RFs. If the positive arrival at about 7 s or that at about 10 s after the direct *P*-wave (Figures 4 and 7) represents the bottom of the underplated layer, the corresponding thickness of the layer would be 40 or 80 km, which would lead to a *P*-wave travel time delay of 0.7 or 1.4 s, respectively under the assumption that V_p (about 7.1 km/s)of the layer is the same as that observed elsewhere such as the East Greenland rifted margin [*Voss and Jokat*, 2007] and the southwest United States [*Snelson et al.*, 2005]. Such a large travel time delay was not observed by the short-period seismic profile across this region [*Ayadi et al.*, 2000]. Indeed, a recent seismic refraction survey found that beneath the passive margin in Greenland, which is most likely a more favorable locale than the study area for magmatic underplating, the thickness of the underplated layer is only about 15 km [*Voss and Jokat*, 2007]. Therefore, the arrivals at 7 and 10 s on the RFs (Figures 4 and 7) are unlikely *P*-to-*S* converted phases from the bottom of the underplated layer which is likely a layer thinner than 10 km. Instead, the arrivals could reflect internal layering of the lithosphere such as the Hales discontinuity [*Hales*, 1969].

4.2. Effects of Crustal Strength on Magmatic Movement

[27] As summarized by *Baer and Reches* [1991], the level at which the rising magma stops is dependent on a number of factors, such as the hydrostatic stress, the excessive pressure within the magma chamber due to magma differentiation and consequent oversaturation of water, resistance to magma flow due to viscous pressure drop, direction and magnitude of tectonic stress, elastic resistance by surrounding rocks to the rising magma which push dike walls apart, and finally, strength of the host rock layers in resisting brittle fracturing at the tip of the propagating dike. The effects of those factors on the depth and shape of igneous intrusion have been investigated by numerous studies [e.g., *Hogan and Gilbert*, 1995]. Obviously, a mechanically weaker and/or more fractured crust makes it easier for magma to rise to the surface than a mechanically stronger, less fractured crust.

[28] When the driving pressure is insufficient for the magma to push through the overlying rock layers, the magma spreads horizontally in zones of sudden changes in density [*Cox*, 1993]. The crust/mantle boundary is a favorable region for temporary or permanent magma storage, because 1) the overlying crust has a 20% reduction in density and thus a reduction in hydrostatic stress which reduces the upward magma driving force; 2) the *Moho* is a mechanical discontinuity. Such magmatic underplating beneath the *Moho* was suggested in many areas such as large igneous provinces [*Xu and He*, 2007], continental rifts [*Keller et al.*, 1994], and the southwest United States [*Snelson et al.*, 2005].

[29] The above factors can explain the difference in volcanism and the observed difference in *R* between the Tefedest and the Laouni terranes. If we assume that both terranes underwent the same tectonic stress field during the period when the brittle fracture system was formed, the significantly better developed fracture system in the Tefedest terrane (Figure 2) suggests that it has a mechanically weaker crust. Alternatively, if we assume that the crust beneath both terranes initially had the same strength and the more developed fracture system in the Tefedest was the result of a strong stress field, a mechanically weaker crust beneath the Tefedest was developed by the fractures.

[30] Under the reasonable assumption that the magma driving forces are the same beneath both terranes, the weaker and fractured Tefedest crust facilitates diking and eruption of the magma to

the surface without being trapped in horizontal layers of weakness; on the other hand, the strong Laouni crust may trap the magma beneath the *Moho* (Figure 11). This scenario can explain the dramatic asymmetry in both surface distribution of volcanism (Figure 2) and the observed effectiveness of the *Moho* in producing P_xS (Figure 9). The larger V_p/V_s values observed in the Tefedest terrane (Figures 8 and 9), and the slightly higher crustal velocity beneath the terrane [*Ayadi et al.*, 2000] can also be explained in terms of the mafic dikes in the Tefedest crust and the layer of basaltic rocks on the surface.

4.3. Constraints on the Depth of Magma Source

[31] The depth range of the magma source of the Cenozoic volcanism on Hoggar is still a controversial issue. Some of the proposed estimates include 20–70 km with a maximum thickness of 30 km [*Lesquer et al.*, 1988], shallower than 60 km [*Crough*, 1981], deeper than 60 km [*Brown and Girdler*, 1980], in the shallow mantle (>35 km) associated with rejuvenation of Pan-African structures [*Liegeois et al.*, 2005], and in the deep mantle fed by a mantle plume [*Sleep*, 1990].

[32] Our V_p/V_s measurements (Figures 8 and 9) are inconsistent with a mafic body in the crust, which would significantly elevate the V_p/V_s observations. For instance, for a crust of 35 km thick composed by a 20 km thick "original" crust with a V_p/V_s of 1.75 and a 15-km-thick layer of gabbro with a V_p/V_s of 1.87 [*Tarkov and Vavakin*, 1982], the resulting overall V_p/V_s is about 1.80. Because the reduction in V_s is greater than that in V_p in totally or partially molten rocks, a magmatic body in the crust would further increase the V_p/V_s values. Additionally, a magma chamber in the crust would lead to complicated waveforms in the RFs, including a negative arrival in the time window of 0 to ~4.3 s. Such complexity is not observed in the RFs (Figure 4). Therefore, it is unlikely that the magma source resides in the crust.

[33] In principle the inferred underplated magmatic layer beneath the Laouni terrane could be the source for the volcanic eruptions on the Tefedest terrane. This scenario is unlikely for several reasons. First, it is reasonable to assume that areas closer to the source region would experience more volcanic activity, yet the anticipated decrease in volcanic activities and the associated decrease in V_p/V_s (due to decrease in diking intensity) observations toward the northwest on the Tefedest terrane are not observed. Second, the NE-SW main fault, which is a zone of weakness and is located right on the edge of the source region, should be a favored locale for eruptions. The anticipated chain of volcanoes along the fault is not observed. Instead, the fault serves as a sharp boundary of the volcanism on the Tefedest terrane. Third, this model requires (sub)horizontal northwestward magmatic migration. Because the *Moho* is a zone of mechanical discontinuity and thus is a zone of weakness, magma may migrate in a horizontal channel in the vicinity of the *Moho*. This channel would reduce the *R* values by reducing the velocity contrast across the *Moho* and by modulating *Moho* topography beneath the Tefedest terrane. In addition, it would also lead to a northwestward increase in the *R* measurements in the terrane due to reduced thickness of the channel away from the source region. Both anticipated characteristics of *R* are not observed. Instead, we see a sharp *Moho* without any indication of a northwestward increase in the *R* observations (Figure 9).

[34] Therefore, our results favor a mantle magma source with a considerable distance from the *Moho*, probably deeper than the maximum vertical extent of the fault that separates the Tefedest and Laouni terranes. This is consistent with the results of *Gangopadhyay et al.* [2007] who suggested an approximately 10% reduction of *P*-wave velocity at a depth of 80 km beneath TAM, extending to at least 100 km.

5. Conclusions

[35] The main conclusion from the systematic analyses of 20 years of broadband seismic data recorded by station TAM on the Hoggar swell is that the volcanic, highly-fractured Tefedest terrane is characterized by an intermediate-mafic crust that is separated from the mantle by a sharp *Moho*. On the contrary, the felsic crust of the non-volcanic, mechanically stronger Laouni terrane is underlain by a magmatic layer which reduces the velocity contrast across the *Moho* and causes spatially variable *Moho* topography. The relatively more mafic crust beneath the Tefedest terrane is likely the consequence of the presence of mafic dikes. The analyses also favor a mantle source for the Cenozoic volcanism.

[36] The study demonstrates the great potential of a single long-running seismic station in the investigation of small-scale spatial variations in crustal characteristics in the vicinity of the station, and could lay the foundation for a multi-station broad-

band seismic experiment aimed at a greatly improved understanding of the formation, structure, and evolution of the intriguing Hoggar and other volcanic swells in northwest Africa.

Acknowledgments

[37] Data used for the study were recorded by a seismic station in the GEOSCOPE network, and were obtained from the IRIS DMC. Comments by E. Sandvol, an anonymous reviewer and an anonymous associate editor, and Editor T. Becker greatly improved the manuscript. We thank Annie Gao for illustrating Figures 2 and 11. The study was partially funded by NSF awards EAR-0703359 and EAR-0911346.

References

Ammon, C. J., G. E. Randall, and G. Zandt (1990), On the non-uniqueness of receiver function inversions, *J. Geophys. Res.*, *95*, 15,303–15,318.

Assouni-Sekkal, A., B. Bonin, A. Benhallou, R. Yahiaoui, and J.-P. Liegeois (2007), Cenozoic alkaline volcanism of the Atakor massif, Hoggar, Algeria, in *Cenozoic Volcanism in the Mediterranean Area*, edited by L. Beccaluva, G. Bianchini, and M. Wilson, *Spec. Pap. Geol. Soc. Am.*, *418*, 321–340.

Ayadi, A., C. Dorbath, A. Lesquer, and M. Bezzeghoud (2000), Crustal and upper mantle velocity structure of the Hoggar swell Central Sahara, Algeria, *Phys. Earth Planet. Inter.*, *118*, 111–123.

Baer, G., and Z. Reches (1991), Mechanics of emplacement and tectonic implications of the Ramon dike systems, Israel, *J. Geophys. Res.*, *96*, 11,895–11,910.

Ball, E. (1980), An example of very consistent brittle deformation over a wide intracontinental area: The late Pan-African fracture system of the Tuareg and Nigerian shield, *Tectonophysics*, *61*, 363–379, doi:10.1016/00401951(180)90240-1.

Beccaluva, L., A. Azzouni-Sekkal, A. Benhallou, G. Bianchini, R. M. Ellam, M. Marzola, F. Siena, and F. M. Stuart (2007), Intracratonic asthenosphere upwelling and lithosphere rejuvenation beneath the Hoggar swell (Algeria): Evidence from HIMU metasomatised lherzolite mantle xenoliths, *Earth Planet. Sci. Lett.*, *260*, 482–494.

Begg, G. C., et al. (2009), The lithospheric architecture of Africa: Seismic tomography, mantle petrology, and tectonic evolution, *Geosphere*, *5*, 23–50.

Black, R., L. Latouche, J. P. Liegeois, R. Caby, and J. M. Bertrand (1994), Pan-African displaced terranes in the Tuareg shield (central Sahara), *Geology*, *22*, 641–644.

Brown, C., and R. W. Girdler (1980), Interpretation of African gravity and its implication for the breakup of the continents, *J. Geophys. Res.*, *85*, 6443–6455.

Burke, K. (1996), The African plate, *S. Afr. J. Geol.*, *99*, 339–410.

Christensen, N. I. (1996), Poisson's ratio and crustal seismology, *J. Geophys. Res.*, *101*, 3139–3156.

Cox, K. G. (1993), Continental magmatic underplating, *Philos. Trans. Phys. Sci. Eng.*, *342*, 155–166.

Crough, S. T. (1981), Free-air gravity over the Hoggar massif, northwest Africa: Evidence for the alteration of the lithosphere, *Tectonophysics*, *77*, 189–202, doi:10.1016/0040-1951(181)90262-6.

Doucoure, C. M., and M. J. de Wit (2003), Old inherited origin for the present near-bimodal topography of Africa, *J. Afr. Earth Sci.*, *36*, 371–388, doi:10.1016/S0899-5362(03)00019-8.

Durrheim, R. J., and R. W. Green (1992), A seismic refraction investigation of the Archaean Kaapvaal Craton, South Africa, using mine tremors as the energy source, *Geophys. J. Int.*, *108*, 812–832.

Efron, B., and R. Tibshirani (1986), Bootstrap methods for standard errors, confidence intervals, and other measures of statistical accuracy, *Stat. Sci.*, *1*, 54–77.

Garnero, E. J., T. Lay, and A. K. McNamara (2007), Implications of lower mantle structural heterogeneity for existence and nature of whole mantle plumes, in *Plates, Plumes, and Planetary Processes*, edited by G. R. Foulger and D. M. Jurdy, *Spec. Pap. Geol. Soc. Am.*, *430*, 79–101.

Gangopadhyay, A., J. Pulliam, and M. K. Sen (2007), Waveform modeling of teleseismic *S,Sp,SsPmP*, and shear-coupled *PL* waves for crust-and upper-mantle velocity structure beneath Africa, *Geophys. J. Int.*, *170*, 1210–1226.

Grand, S. (2002), Mantle shear-wave tomography and the fate of subducted slabs, *Philos. Trans. R. Soc. London, Ser. A*, *360*, 2475–2491.

Hales, A. L. (1969), A seismic discontinuity in the lithosphere, *Earth Planet. Sci. Lett.*, *7*, 44–46, doi:10.1016/0012-821X(69)90009-0.

Hogan, J. P., and M. C. Gilbert (1995), The A-type Mount Scott Granite Sheet: Importance of crustal magma traps, *J. Geophys. Res.*, *100*, 15,779–15,793.

Keller, G. R., et al. (1994), The East African rift system in the light of KRISP 90, *Tectonophysics*, *236*, 465–483.

Lesquer, A., A. Bourmatte, and J. M. Dautria (1988), Deep structure of the Hoggar domal uplift (Central Sahara, south Algeria) from gravity, thermal and petrological data, *Tectonophysics*, *152*, 71–87.

Lesquer, A., A. Bourmatte, S. Ly, and J. M. Dautria (1989), First heat flow determination from the Central Sahara: Relationship with the Pan-African belt and Hoggar domal uplift, *J. Afr. Earth Sci.*, *9*, 41–48, doi: 10.1016/0899-5362(89)90006-7.

Liegeois, J.-P., L. Latouche, B. Mustapha, J. Navez, and M. Guiraud (2003), The LATEA metacraton (Central Hoggar, Tuareg shield, Algeria): Behaviour of an old passive margin during the Pan-African orogeny, *J. Afr. Earth Sci.*, *37*, 161–190.

Liegeois, J.-P., A. Benhallou, A. Azzouni-Sekkal, R. Yahiaoui, and B. Bonin (2005), The Hoggar swell and volcanism: Reactivation of the Precambrian Tuareg shield during Alpine convergence and West African Cenozoic volcanism, *Spec. Pap. Geol. Soc. Am.*, *388*, 379–400.

Nair, S. K., S. S. Gao, K. H. Liu, and P. G. Silver (2006), Southern African crustal evolution and composition: Constraints from receiver function studies, *J. Geophys. Res.*, *111*, B02304, doi:10.1029/2005JB003802.

Peucat, J. J., A. Drareni, L. Latouche, E. Deloule, and P. Vidal (2003), U-Pb zircon (TIMS and SIMS) and Sm-Nd whole-rock geochronology of the Gour Oumelalen granulitic basement, Hoggar massif, Tuareg shield, Algeria, *J. Afr. Earth Sci.*, *37*, 229–239.

Poppeliers, C., and T. Datta (2010), The effects of crustal heterogeneity on ray-based teleseismic imaging, *Geophys. J. Int.*, *181*, 1041–1061, doi: 10.1111/j.1365-246X.2010. 04555.x.

Press, W. H., S. A. Teukolsky, W. T. Vetterling, and B. P. Flannery (1992), *Numerical Recipes in FORTRAN*, 2nd ed., Cambridge Univ. Press, Cambridge, U. K.

Sandvol, E., D. Sebeer, A. Calvert, and M. Barazangi (1998), Grid search modeling of receiver functions: Implications for crustal structure in the Middle East and North Africa, *J. Geophys. Res.*, *103*, 26,899–26,917.

Sleep, N. H. (1990), Hotspots and mantle plumes: Some phenomenology, *J. Geophys. Res.*, *95*, 6715–6736.

Snelson, C. M., G. R. Kelly, K. C. Miller, H.-M. Rumpel, and C. Prodehl (2005), Regional crustal structure derived from the CD-ROM 99 seismic refraction/wide-angle reflection profile: The lower crust and upper mantle, in *The Rocky Mountain Region: An Evolving Lithosphere*, *Geophys. Monogr. Ser.*, vol. 154, pp. 271–291, AGU, Washington, D. C.

Tapley, B., et al. (2005), GGM02—An improved Earth gravity field model from GRACE, *J. Geod.*, *79*, 467–478, doi:10.1007/s00190-005-0480-z.

Tarkov, A. P., and V. V. Vavakin (1982), Poisson's ratio behavior in various crystalline rocks: Application to the study of the Earth's interior, *Phys. Earth Planet. Inter.*, *29*, 24–29.

Voss, M., and W. Jokat (2007), Continent-ocean transition and voluminous magmatic underplating derived from *P*-wave velocity modeling of the East Greenland continental margin, *Geophys. J. Int.*, *170*, 580–604, doi:10.1111/j.1365-246X.2007.03438.x.

Xu, Y., and B. He (2007), Thick, high-velocity crust in the Emeishan large igneous province, southwestern China: Evidence for crustal growth by magmatic underplating or intraplating, in *Plates, Plumes, and Planetary Processes*, edited by G. R. Foulger and D. M. Jurdy, *Spec. Pap. Geol. Soc. Am.*, *430*, 841–858.

Zhu, L. P., and H. Kanamori (2000), *Moho* depth variation in southern California from teleseismic receiver functions, *J. Geophys. Res.*, *105*, 2969–2980.